

OccMamba: Semantic Occupancy Prediction with State Space Models

Heng Li¹, Yuenan Hou^{2*}, Xiaohan Xing³, Xiao Sun², Yanyong Zhang^{1*}

¹ University of Science and Technology of China, ² Shanghai AI Laboratory, ³ Stanford University
li_heng@mail.ustc.edu.cn, houyuenan@pjlab.org.cn, xhxing@stanford.edu, sunxiao@pjlab.org.cn, yanyongz@ustc.edu.cn

Abstract

Training deep learning models for semantic occupancy prediction is challenging due to factors such as a large number of occupancy cells, severe occlusion, limited visual cues, complicated driving scenarios, etc. Recent methods often adopt transformer-based architectures given their strong capability in learning input-conditioned weights and long-range relationships. However, transformer-based networks are notorious for their quadratic computation complexity, seriously undermining their efficacy and deployment in semantic occupancy prediction. Inspired by the global modeling and linear computation complexity of the Mamba architecture, we present the first Mamba-based network for semantic occupancy prediction, termed OccMamba. However, directly applying the Mamba architecture to the occupancy prediction task yields unsatisfactory performance due to the inherent domain gap between the linguistic and 3D domains. To relieve this problem, we present a simple yet effective 3D-to-1D reordering operation, i.e., height-prioritized 2D Hilbert expansion. It can maximally retain the spatial structure of point clouds as well as facilitate the processing of Mamba blocks. Our OccMamba achieves state-of-the-art performance on three prevalent occupancy prediction benchmarks, including OpenOccupancy, SemanticKITTI and SemanticPOSS. Notably, on OpenOccupancy, our OccMamba outperforms the previous state-of-the-art Co-Occ by **3.1%** IoU and **3.2%** mIoU, respectively. Codes will be released upon publication.

1 Introduction

Semantic occupancy prediction is becoming an indispensable component in autonomous driving, augmented reality, robotics (Roldao, De Charette, and Verroust-Blondet 2022), etc., which estimates the occupancy and categorical labels of the surrounding environment. It faces many challenges, such as the enormous number of occupancy grids, severe occlusion, limited visual clues as well as complex driving scenarios (Zhang et al. 2024b).

Recent attempts, such as MonoScene (Cao and De Charette 2022) and JS3C-Net (Yan et al. 2021), have made progress in addressing these challenges, but limitations remain due to their reliance on uni-modal inputs. Multi-modal approaches, such as FusionOcc (Zhang et al.

2024a) and M-CONet (Wang et al. 2023b), offer improvements, yet they struggle to capture global information due to the inherent deficiency of CNN architectures. Despite the success of transformer-based models (Li et al. 2023b; Tong et al. 2023; Zhang, Zhu, and Du 2023), they suffer from high computational complexity, particularly when processing a large number of voxel grids.

Mamba (Gu and Dao 2023), which is an important variant of state space models, emerges as a promising next-generation structure for replacing the transformer architecture. In semantic occupancy prediction, we anticipate leveraging its global modeling capabilities to better handle the complex scenarios and overcome limited visual cues, while its linear computation complexity helps manage the enormous number of occupancy grids efficiently. However, it is primarily designed for language modeling, with 1D input data, whereas the input data for semantic occupancy prediction is 3D voxels. The use of dense voxels in large scenes makes the deployment of Mamba even more challenging. When converting 3D data into a 1D format, the inherent spatial relationships between adjacent voxels in the 3D space are missing, causing neighboring voxels to become far apart in the 1D sequence. This spatial separation undermines Mamba’s ability to effectively understand local and global scene contexts, hampering the prediction performance. To address this issue, developing an effective reordering strategy is crucial to preserving spatial proximity in the transformation from 3D to 1D. Several attempts have been made to the design of such a reordering policy. For instance, Point Mamba (Liang et al. 2024) rearranges the point clouds according to the 3D Hilbert curve (Hilbert 2013) and concatenates the features of the reordered points. While these advancements have shown potential in the point cloud classification and segmentation field, the exploration of Mamba-based architectures is still in its infancy in outdoor semantic occupancy prediction tasks.

In this work, we present the first Mamba-based network for semantic occupancy prediction, which we refer to as OccMamba. Owing to the global modeling and linear computation complexity of Mamba, our OccMamba can efficiently process a large number of voxel grids given limited computation resources, as shown in Fig. 1(a)-(b). To facilitate the processing of Mamba blocks as well as preserve the spatial structure of the 3D input data, we present a simple yet effective

* The corresponding authors.

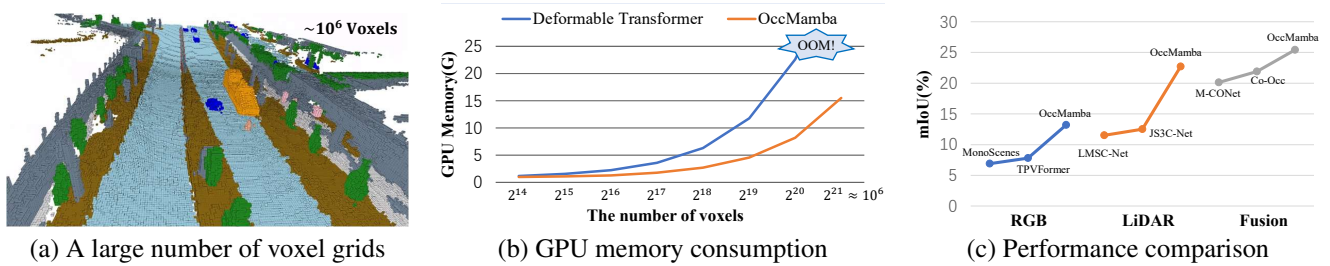


Figure 1: (a) Challenges in semantic occupancy prediction, (b) comparison in GPU memory consumption, and (c) performance comparison on OpenOccupancy validation set. Our OccMamba demonstrates high efficiency in handling a large number of voxel grids, outperforming all other semantic occupancy predictors, such as TPVFormer (Huang et al. 2023) and M-COCC (Wang et al. 2023b) under the settings of RGB-only, LiDAR-only and multi-modal fusion.

tive 3D-to-1D reordering policy, i.e., height-prioritized 2D Hilbert expansion. The designed policy sufficiently utilizes the categorical clues in the height information as well as the spatial prior in the XY plane. In this way, OccMamba effectively exploits LiDAR and camera cues, enabling effective fusion and processing of voxel features extracted from these sources without compression. This uncompressed voxel feature processing method, combined with Mamba’s global modeling capabilities, enhances OccMamba with the occlusion reasoning capability, particularly in complex driving scenarios. We perform extensive experiments on three semantic occupancy prediction benchmarks, i.e., OpenOccupancy (Wang et al. 2023b), SemanticKITTI (Behley et al. 2019) and SemanticPOSS (Pan et al. 2020). Our OccMamba consistently outperforms state-of-the-art algorithms in all benchmarks. It is noteworthy that on OpenOccupancy, partly shown in Fig. 1(c), our OccMamba surpasses the previous state-of-the-art Co-Occ (Pan, Wang, and Wang 2024) by **3.1% IoU** and **3.2% mIoU**, respectively.

The contributions of our paper are summarized as follows:

- To the best of our knowledge, we design the first Mamba-based network for outdoor semantic occupancy prediction. It possesses global modeling capability with linear computation complexity, which is essential to the processing of a large number of occupancy grids.
- To facilitate the processing of Mamba blocks as well as maximally retain the original spatial structure of point clouds, we design a simple yet effective reordering policy that projects the point clouds into 1D sequences.
- Our OccMamba achieves the best performance on three popular semantic occupancy prediction benchmarks.

2 Related work

Semantic Occupancy Prediction. The objective of semantic occupancy prediction is to estimate the occupancy and semantic labels of 3D spaces using various types of input signals (Roldao, De Charette, and Verroust-Blondet 2022). Given that LiDAR and RGB-D camera can provide accurate spatial measurement, many studies relied on such detailed geometric data like LiDAR points (Rist et al. 2021; Xia et al. 2023; Roldao, de Charette, and Verroust-Blondet 2020; Yan et al. 2021) and RGB-D images (Chen et al. 2020; Li et al.

2020a; Garbade et al. 2019; Li et al. 2020b). Meanwhile, image-based methods, increasingly popular due to camera accessibility, such as MonoScene (Cao and De Charette 2022) and TPVFormer (Huang et al. 2023), estimate occupancy of the environment using RGB images. However, inaccurate depth estimation in RGB images results in lower performance than LiDAR-based models. In response, multi-modal fusion combining both modalities has attracted significant attention. CONet (Wang et al. 2023b) and Co-Occ (Pan, Wang, and Wang 2024) demonstrate the advantages of combining modalities, enhancing precision and reliability. Furthermore, recent methods have shifted from CNNs to integrating transformers, as seen in OccFormer’s dual-path transformer (Zhang, Zhu, and Du 2023) and OccNet’s cascade refinement (Tong et al. 2023) reduce the transformer’s computational demands.

Multi-Modal Fusion. Multi-modal fusion aims to make the strength of different input modalities, thus making more accurate and robust perception (Gao et al. 2020; Li et al. 2020a; Liu et al. 2023; Wang et al. 2023a). For instance, AICNet (Li et al. 2020a) integrates RGB and depth data using anisotropic convolutional networks to enhance the accuracy and completeness of semantic occupancy prediction. PointPainting (Vora et al. 2020) performs semantic segmentation on RGB images and attaches semantic probabilities to LiDAR points, thereby enriching the point cloud with rich semantic information. For semantic occupancy prediction, images and point clouds are two prevalent input signals. Recent trends in the occupancy prediction field favour the multi-modal fusion as it utilizes the strength of both signals.

State Space Models. The transformer (Vaswani et al. 2017) has reshaped the computer vision field but suffers from the quadratic computation complexity (Lin et al. 2022). To relieve this, more efficient operators like linear attention (Wang et al. 2020), flash attention (Dao et al. 2022) have been proposed. State space model series (SSMs) such as Mamba (Gu and Dao 2023), S4 (Gu, Goel, and Ré 2021), and S4nd (Nguyen et al. 2022) are gaining prominence, with Mamba being notable for integrating selective mechanisms, which can effectively capture long-range dependencies and process large-scale data in linear time. This innovation has extended into computer vision domain through variants like VMamba (Liu et al. 2024b), which includes a

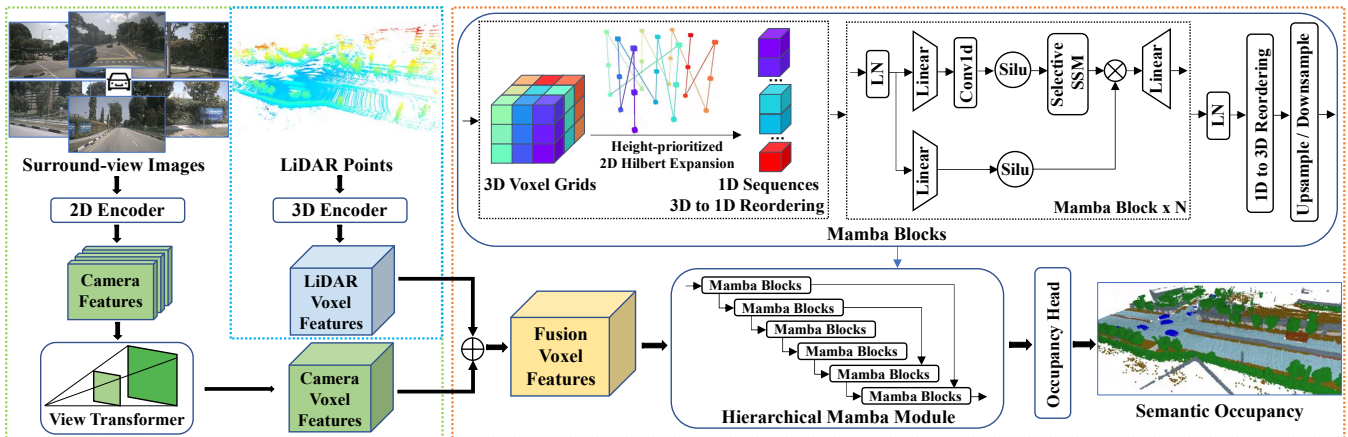


Figure 2: Schematic overview of our OccMamba. Given surround-view images and LiDAR point clouds, we first employ 2D encoder and 3D encoder to process them and obtain camera features and LiDAR voxel features, respectively. View transformer is utilized to project 2D camera features into 3D space, producing camera voxel features. Camera voxel features and LiDAR voxel features are fused and sent to the hierarchical Mamba module, where the proposed height-prioritized 2D Hilbert expansion reordering scheme is used to maximally utilize the spatial clues of voxels. Eventually, the Mamba features are fed to the occupancy head, producing semantic occupancy predictions.

cross-scan module, and Vision Mamba (Zhu et al. 2024), which utilizes a bidirectional SSM. In point cloud processing, PointMamba (Liang et al. 2024) improves the global modeling of point clouds by rearranging input patches based on 3D Hilbert curve, while Point Mamba (Liu et al. 2024a) employs an octree-based ordering for efficient spatial relationship capture. These developments demonstrate Mamba’s proficiency in processing large scale 3D data. Building on these advancements, we attempt to design a Mamba-based network tailored for semantic occupancy prediction.

3 Methodology

To efficiently and effectively process a large number of voxel grids in semantic occupancy prediction, we propose to take Mamba (Gu and Dao 2023) as the basic building block that enjoys the benefit of both global modeling and linear computation complexity. To facilitate the processing of Mamba blocks, we design a simple yet effective reordering scheme, dubbed height-prioritized 2D Hilbert expansion, along with the Hierarchical Mamba Encoder and Decoder. In the following sections, we first provide a brief review of state space models and Mamba in Sec. 3.1. Then, we present the framework overview of OccMamba in Sec. 3.2. Thereafter, we provide a detailed explanation of the reordering scheme, the hierarchical Mamba encoder and decoder in Sec. 3.3. Eventually, the training objective is presented in Sec. 3.4.

3.1 Preliminaries

State Space Models. Before introducing the Mamba module, we first have a brief review of the state space models (SSMs). SSMs are inspired by the control theory and maps the system input to the system output through the hidden state. This approach allows for effectively handling sequences of information. When the input is discrete, the mathematical representation of SSMs is given as follows:

$$\begin{aligned} h_k &= \bar{A}h_{k-1} + \bar{B}x_k, \\ y_k &= \bar{C}h_k, \end{aligned} \quad (1)$$

where k is the sequence number, \bar{A} , \bar{B} , \bar{C} are matrices that represent the discretized parameters of the model, which involve the sampling step Δ . The x_k , y_k , and h_k denote the input, output, and hidden state of the system, respectively. Structure state space sequence models (S4) (Gu, Goel, and Ré 2021) introduces a new parameterization for SSMs to achieve more efficient computation.

Mamba Module. Mamba introduces an adaptation to the S4 models (Gu, Goel, and Ré 2021), where it makes the matrices \bar{B} and \bar{C} , as well as the sampling size Δ , dependent on the input. This dependency arises from incorporating the sequence length and batch size of the input, enabling dynamic adjustments of these matrices for each input token. By this way, Mamba allows \bar{B} and \bar{C} to dynamically influence the state transition conditioned on the input, enhancing the model’s content-awareness.

3.2 Framework Overview

Figure 2 depicts the pipeline of our OccMamba, which is built upon M-CONet (Wang et al. 2023b).

Multi-Modal Visual Encoders. Taking both point cloud and multi-view images as input, OccMamba processes each modality with respective visual encoder. Specifically, for the LiDAR branch, we first voxelize the input point clouds \mathbf{P} (Zhou and Tuzel 2018) and then employ sparse-convolution-based LiDAR encoder $\mathbf{E}_{\mathcal{L}}$ (Yan, Mao, and Li 2018) to generate LiDAR voxel features $\mathbf{V}_{\mathcal{L}} \in \mathbb{R}^{W_{\mathcal{L}} \times H_{\mathcal{L}} \times D_{\mathcal{L}} \times C_{\mathcal{L}}}$. For the image branch, we feed the multi-view images \mathbf{I} to ResNet-based image encoder (He et al. 2016) which utilizes FPN (Lin et al. 2017) to aggregate multi-scale features, and then utilize the 2D-to-3D view

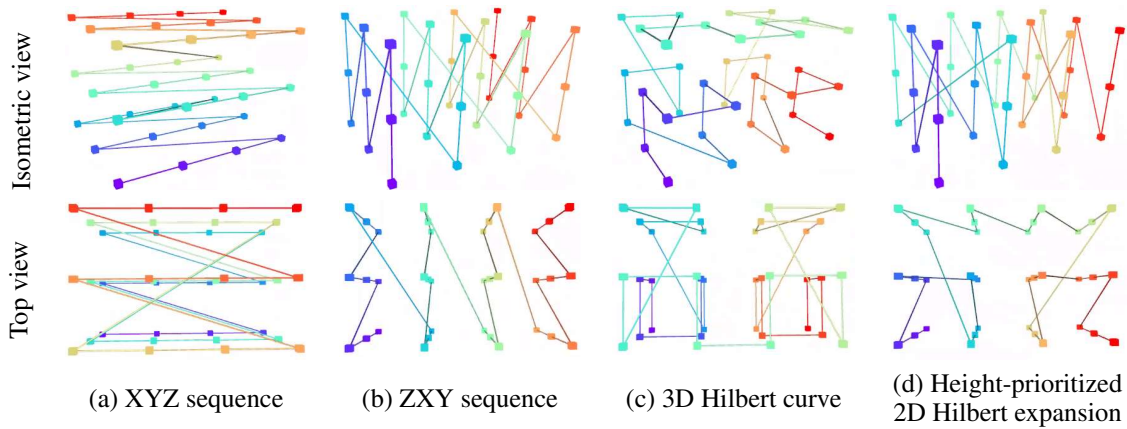


Figure 3: Comparison between different reordering schemes. (a) XYZ sequence, (b) ZXY sequence, (c) 3D Hilbert curve, and (d) our height-prioritized 2D Hilbert expansion. Small cubes of varying colors, ranging from red to purple, represent different voxels. The corresponding colored edges indicate the adjacency of voxels that become neighbors after reordering. In each sub-figure, its top half represents the isometric view, and the bottom half represents the top view. Our method maximizes z-axis proximity while also striving to preserve xy-axis proximity.

transformer (Liu et al. 2023) to produce image voxel features $\mathbf{V}_C \in \mathbb{R}^{W_C \times H_C \times D_C \times C_C}$. Here, W_C , H_C , D_C and C_C are the spatial dimensions of the voxel features. W_L and C_L are the channel dimension of these voxel features. We ensure that \mathbf{V}_L and \mathbf{V}_C are identical in the spatial dimensions. Thereafter, we perform concatenation on these voxel features along the channel dimensions:

$$\mathbf{V} = \text{concat}(\mathbf{V}_L, \mathbf{V}_C). \quad (2)$$

To process features extracted from the multi-modal encoders, we design the Mamba Encoder \mathbf{E}_M and Mamba Decoder \mathbf{D}_M as integral parts of our entire Mamba Module. In the process, voxel features \mathbf{V} are fed into the Mamba module, which will be detailed in Sec. 3.3. The transformation can be described by

$$\mathbf{V}' = \mathbf{D}_M(\mathbf{E}_M(\mathbf{V})), \quad (3)$$

where \mathbf{V}' retains the same size as \mathbf{V} .

Occupancy Head. We feed the processed features of Mamba blocks, i.e., \mathbf{V}' , to the coarse-to-fine module $\mathbf{F}_{c \rightarrow f}$ (Wang et al. 2023b), which interpolates the dimensions to match the size of the ground truth, and then employ a MLP to predict the category of each voxel grid. The process is presented in the following equation:

$$\mathbf{O}_{\text{occ}} = \text{MLP}(\mathbf{F}_{c \rightarrow f}(\mathbf{V}')). \quad (4)$$

3.3 Hierarchical Mamba Module with Height-prioritized Reordering

Semantic occupancy prediction is challenging due to the high dimensionality and density of voxel grids, often involving millions of voxels. Previous methods (Huang et al. 2023; Ma et al. 2024) resort to projection techniques but suffer from information loss. In contrast, Mamba’s linear computational complexity enables direct processing of large

voxel features, avoiding the limitations of deformable attention and convolutional methods, such as the need for key point selection or limited receptive fields.

Height-prioritized Reordering Scheme. Before feeding 3D voxel features into the Mamba block, it’s necessary to reorder them into 1D sequences. A poor reordering strategy can disrupt the intrinsic spatial relationships between adjacent voxels in the 3D space, especially when dealing with a large number of voxel grids, thereby impacting Mamba’s performance. Inspired by the Hilbert curve (Hilbert 2013), we propose a height-prioritized 2D Hilbert expansion, tailored to the flat spatial structure typical of semantic occupancy prediction tasks, where height information provides valuable categorical clues, as it often correlates with object categories, reveals terrain features, and distinguishes different spatial regions in the environment. Specifically, we divide the "xyz" coordinates into the "xy" plane and a "z" dimension. Starting on the xy-plane at $z=0$, the process extends vertically along the z-axis, creating vertical sequences. These sequences are then ordered and interconnected following the 2D Hilbert curve on the xy plane, forming the height-prioritized 2D Hilbert expansion, as illustrated in Fig. 3(d). For comparison, Fig. 3(a)-(c) illustrate the results of reordering according to the 'xyz' sequence, the 'zxy' sequence, and the 3D Hilbert curve, respectively. Our reordering strategy prioritizes z-axis spatial information while maintaining strong spatial proximity in the xy plane. By this way, we can better leverage Mamba’s contextual modeling.

Hierarchical Mamba Encoder and Decoder. To effectively utilize the contextual information across spatial resolutions, we introduce the hierarchical Mamba encoder and decoder. The encoder comprises multiple groups, each with two Mamba blocks and a downsampling operation between groups for multi-scale voxel features. Correspondingly, the Mamba decoder mirrors this structure, utilizing paired Mamba blocks and upsampling operations. The up-

















| Method | Input Modality | | | barrier | bicycle | bus | car | const. veh. | motorcycle | pedestrian | traffic cone | trailer | truck | drive surf. | other_flat | sidewalk | terrain | manmade | vegetation |
|------------------------|----------------|-------------|-------------|---|---|---|---|---|---|---|---|---|---|---|---|---|---|---|---|
| | | IoU | mIoU |  |  |  |  |  |  |  |  |  |  |  |  |  |  |  |  |
| MonoScene | C | 18.4 | 6.9 | 7.1 | 3.9 | 9.3 | 7.2 | 5.6 | 3.0 | 5.9 | 4.4 | 4.9 | 4.2 | 14.9 | 6.3 | 7.9 | 7.4 | 10.0 | 7.6 |
| TPVFormer | C | 15.3 | 7.8 | 9.3 | 4.1 | 11.3 | 10.1 | 5.2 | 4.3 | 5.9 | 5.3 | 6.8 | 6.5 | 13.6 | 9.0 | 8.3 | 8.0 | 9.2 | 8.2 |
| 3DSketch | C&D | 25.6 | 10.7 | 12.0 | 5.1 | 10.7 | 12.4 | 6.5 | 4.0 | 5.0 | 6.3 | 8.0 | 7.2 | 21.8 | 14.8 | 13.0 | 11.8 | 12.0 | 21.2 |
| AICNet | C&D | 23.8 | 10.6 | 11.5 | 4.0 | 11.8 | 12.3 | 5.1 | 3.8 | 6.2 | 6.0 | 8.2 | 7.5 | 24.1 | 13.0 | 12.8 | 11.5 | 11.6 | 20.2 |
| LMSCNet | L | 27.3 | 11.5 | 12.4 | 4.2 | 12.8 | 12.1 | 6.2 | 4.7 | 6.2 | 6.3 | 8.8 | 7.2 | 24.2 | 12.3 | 16.6 | 14.1 | 13.9 | 22.2 |
| JS3C-Net | L | 30.2 | 12.5 | 14.2 | 3.4 | 13.6 | 12.0 | 7.2 | 4.3 | 7.3 | 6.8 | 9.2 | 9.1 | 27.9 | 15.3 | 14.9 | 16.2 | 14.0 | 24.9 |
| M-CONet | C&L | 29.5 | 20.1 | 23.3 | 13.3 | 21.2 | 24.3 | 15.3 | 15.9 | 18.0 | 13.3 | 15.3 | 20.7 | 33.2 | 21.0 | 22.5 | 21.5 | 19.6 | 23.2 |
| Co-Occ | C&L | 30.6 | 21.9 | 26.5 | <u>16.8</u> | <u>22.3</u> | <u>27.0</u> | 10.1 | <u>20.9</u> | <u>20.7</u> | <u>14.5</u> | 16.4 | <u>21.6</u> | <u>36.9</u> | 23.5 | <u>25.5</u> | 23.7 | 20.5 | 23.5 |
| OccMamba (ours) | C | 21.7 | 13.2 | 13.2 | 7.4 | 15.3 | 17.6 | 6.1 | 10.3 | 10.3 | 6.5 | 6.2 | 13.3 | 32.9 | 20.5 | 19.8 | 17.4 | 4.8 | 8.7 |
| OccMamba (ours) | L | 36.4 | <u>22.7</u> | <u>26.8</u> | 11.3 | 20.8 | 26.1 | <u>14.6</u> | 16.3 | 20.3 | 14.0 | <u>17.5</u> | 20.3 | 39.5 | <u>24.9</u> | 25.9 | 25.3 | 28.3 | 30.6 |
| OccMamba (ours) | C&L | <u>33.7</u> | 25.1 | 29.6 | 20.2 | 25.7 | 28.5 | 16.7 | 25.0 | 23.2 | 19.9 | 20.3 | 24.5 | 36.1 | 25.3 | 25.1 | 24.8 | <u>27.7</u> | <u>28.9</u> |

Table 1: Quantitative comparisons on OpenOccupancy validation set. C, D, L denote camera, depth and LiDAR, respectively. The best and second-best are in bold and underlined, respectively.

sampling operation incorporates skip connection from the corresponding layer in the Mamba encoder, ensuring consistency in feature dimensions across scales. Crucially, the reordering scheme is applied both before and after each Mamba blocks group, maintaining voxel representation during both downsampling and upsampling phases. As to the Mamba block, it consists of LayerNorm(LN), linear layers, 1D convolution, Silu activation, Selective SSM, and residual connections. Given an input $\mathbf{V} \in \mathbb{R}^{\mathcal{B} \times \mathcal{N} \times \mathcal{C}}$, where \mathcal{B} , \mathcal{N} and \mathcal{C} denote the batch size, the number of 1D sequences, and the Mamba feature dimension, respectively, the output \mathbf{V}' can be computed as below:

$$\begin{aligned}
\mathbf{V}'_1 &= \text{LN}(\mathbf{V}), \\
\mathbf{V}'_2 &= \text{Selective SSM}(\text{Silu}(\text{Conv1d}(\text{Linear}(\mathbf{V}'_1))))), \\
\mathbf{V}' &= \text{Linear}(\mathbf{V}'_2 \odot \text{Silu}(\text{Linear}(\mathbf{V}'_1))),
\end{aligned} \quad (5)$$

where \odot represents the dot product.

Endowed with the hierarchical Mamba encoder and decoder, our OccMamba utilizes features at multiple resolutions, thereby leveraging both coarse and fine-grained spatial information. This multi-scale approach preserves low-resolution details, enhancing contextual modeling and mitigating performance degradation with large data volumes.

3.4 Training Objective

Our ultimate training objective is composed of five terms, including the cross-entropy loss \mathcal{L}_{CE} , the lovasz-softmax loss \mathcal{L}_{iou} (Berman, Triki, and Blaschko 2018), the geometric and semantic affinity loss \mathcal{L}_{geo} and \mathcal{L}_{sem} (Cao and De Charette 2022), and the depth supervision loss $\mathcal{L}_{\text{depth}}$ (Li et al. 2023a). These terms are crucial for optimizing our model’s performance in various aspects: \mathcal{L}_{CE} ensures accurate classification, \mathcal{L}_{iou} enhances semantic segmentation, \mathcal{L}_{geo} improves spatial alignment, \mathcal{L}_{sem} refines semantic understanding, and

$\mathcal{L}_{\text{depth}}$ guides depth estimation and spatial relationships. The ultimate training objective is presented as follows:

$$\mathcal{L} = \mathcal{L}_{\text{CE}} + \lambda_1 \mathcal{L}_{\text{iou}} + \lambda_2 \mathcal{L}_{\text{geo}} + \lambda_3 \mathcal{L}_{\text{sem}} + \lambda_4 \mathcal{L}_{\text{depth}}, \quad (6)$$

where $\lambda_1 \sim \lambda_4$ are the loss coefficients to balance the effect of each loss item on the final performance. They are all empirically set to 1.

4 Experiments

4.1 Experimental Setup

Benchmarks. We conduct experiments on OpenOccupancy (Wang et al. 2023b), SemanticKITTI (Behley et al. 2019) and SemanticPOSS (Pan et al. 2020). OpenOccupancy is built upon the nuScenes dataset (Caesar et al. 2020), inheriting the data format of nuScenes. It comprises 700 training sequences and 150 validation sequences, with annotations for 17 classes. The occupancy annotations are represented in a $512 \times 512 \times 40$ voxel grid, with each voxel sized at 0.2 meters. Notably, each frame in OpenOccupancy has a data range four times larger than the other datasets, imposing a heavier computational burden. In SemanticKITTI, sequences 00-10 (excluding 08), 08, and 11-21 are allocated for training, validation, and testing, respectively. For the occupancy annotations, a $256 \times 256 \times 32$ grid is used, with voxels measuring 0.2 meters each. After pre-processing, a total of 19 classes are utilized for training and evaluation. SemanticPOSS, which closely resembles SemanticKITTI, employs sequences 00-05 and 02 as training and validation sets, respectively, with annotations for 11 classes.

Evaluation metrics. We adopt the official evaluation metrics, *i.e.*, Intersection-over-Union (IoU) and mean Intersection-over-Union (mIoU).

Implementation details. We use ResNet-50 (He et al. 2016) as the image backbone. Both the Mamba Encoder and

| Method | Input Modality | IoU | mIoU |
|------------------------|----------------|-------------|-------------|
| M-CO _N et | C&L | 26.8 | 20.5 |
| OccMamba (ours) | C | 21.6 | 13.1 |
| OccMamba (ours) | L | 36.8 | <u>23.1</u> |
| OccMamba (ours) | C&L | <u>36.0</u> | 27.0 |

Table 2: Quantitative comparisons on OpenOccupancy validation set with v0.1 annotations. The best and second-best are in bold and underlined, respectively.

| Method | Input Modality | mIoU |
|-----------------------|----------------|-------------|
| MonoScene | C | 11.1 |
| SurroundOcc | C | 11.9 |
| OccFormer | C | 12.3 |
| RenderOcc | C | 12.8 |
| LMSCNet | L | 17.0 |
| JS3C-Net | L | 23.8 |
| SSC-RS | L | 24.2 |
| Co-Occ | C&L | <u>24.4</u> |
| M-CO _N et | C&L | 20.4 |
| OccMamba(ours) | C&L | 24.6 |

Table 3: Performance on SemanticKITTI test set. The best and second-best are in bold and underlined, respectively.

Mamba Decoder consist of four groups and each group contains two Mamba blocks. For the OpenOccupancy dataset, we maintain identical setting to M-CO_Net (Wang et al. 2023b): for each frame, we utilize six surround view camera images as input, coupled with a fusion of ten frames of LiDAR points spanning the range of [-51.2m, 51.2m] along the X and Y axes, and [-2.0m, 6.0m] along the Z axis. Within the Mamba Module, we set the feature dimension to 384. On the SemanticKITTI dataset, our inputs consist of forward-facing stereo camera images alongside a single-frame LiDAR points, with their spatial extents defined as [0m, -25.6m, -2m, 51.2m, 25.6m, 4.4m]. We set the mamba feature dimension to 128 and employ Test Time Augmentation (TTA) to boost the performance. The used augmentations include the flipping of the X and Y axes, and four augmented inputs (including the original input) are sent to the model. Finally, for the SemanticPOSS dataset, we exclusively leverage single-frame LiDAR points like SemanticKITTI.

4.2 Experimental Results

OpenOccupancy. As shown in Table 1, we compare OccMamba on OpenOccupancy with previous methods under the settings of camera-only (Cao and De Charette 2022; Huang et al. 2023; Chen et al. 2020; Li et al. 2020a), LiDAR-only (Roldao, de Charette, and Verroust-Blondet 2020; Yan et al. 2021), and multi-modal fusion (Wang et al. 2023b; Pan, Wang, and Wang 2024). Our OccMamba achieves the best performance across all settings. Particularly, in the multi-modal fusion, OccMamba outperforms Co-Occ (Pan, Wang, and Wang 2024) by 3.1% in IoU and 3.2% in mIoU, respec-

| Method | mIoU |
|-----------------------|-------------|
| SSCNet | 15.2 |
| LMSCNet | 16.5 |
| MotionSC | 17.6 |
| JS3C-Net | <u>22.7</u> |
| OccMamba(ours) | 23.4 |

Table 4: Comparisons on SemanticPOSS validation set. The best is in bold, and the second-best is underlined.

| Reordering Schemes | mIoU |
|--|-------------|
| XYZ sequence | 25.3 |
| 3D Hilbert | 25.5 |
| ZXY sequence | 25.5 |
| Height-prioritized 2D Hilbert expansion | 25.9 |

Table 5: Ablation study on different reordering schemes.

tively. These results underscore the efficacy of our approach in handling large-scale scenarios. Besides, we also conduct experiments on the newly published v0.1 annotations of OpenOccupancy in Table 2. OccMamba still exhibits competitive performance, achieving an mIoU of 27.0%, which is 6.5% higher than M-CO_Net (Wang et al. 2023b).

SemanticKITTI & SemanticPOSS. As evident from Table 3, our OccMamba still outperforms the second-best method, *i.e.*, Co-Occ (Pan, Wang, and Wang 2024), by 0.2% mIoU in SemanticKITTI test set. Note that we do not compare our OccMamba with SCPNet (Xia et al. 2023) and Oc-cfiner (Shi et al. 2024) as they employ tricks such as label rectification, knowledge distillation or multi-frame concatenation. Strong performance is also observed in SemanticPOSS, as shown in Table 4. These results sufficiently demonstrate the superiority of our approach. The detailed classwise performance is put in the supplementary material.

Visual comparisons. From Fig. 4, our OccMamba produces more accurate predictions than M-CO_Net (Wang et al. 2023b) on OpenOccupancy validation set. Our OccMamba not only provides a more detailed representation of object shapes and semantics, but also performs preciser predictions on occluded objects and surfaces.

4.3 Ablation Study

The reported results are on the OpenOccupancy validation set with v0.1 annotations unless otherwise specified.

Reordering Schemes. To accelerate the training process, we set the mamba feature dimension to 128 and then compare our method with three alternative methods: ordering by XYZ sequence, ordering by ZXY sequence, and ordering using the 3D Hilbert curve. As shown in Table 5, our method achieves the highest mIoU of 25.9%. Additionally, it is apparent that reordering schemes that prioritize the z-axis outperform the other methods. This could be attributed to the fact that in semantic occupancy prediction, the overall shape of the scenes typically manifests as a flattened cuboid.

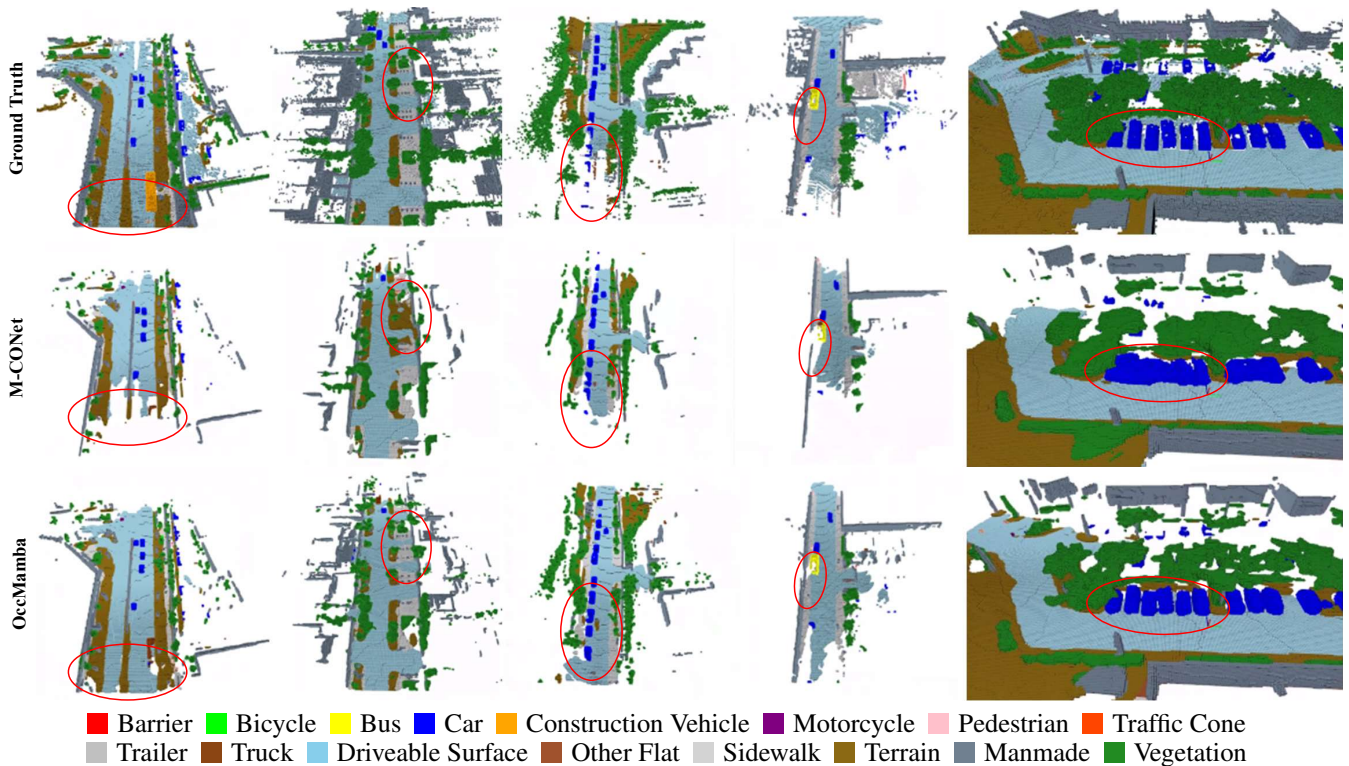


Figure 4: Visual comparison between OccMamba and M-CONet. From top to bottom: ground-truth, predictions of M-CONet and OccMamba. Our OccMamba makes preciser predictions than M-CONet especially in regions highlighted by red ellipses.

| Method | mIoU |
|---------------------------------------|-------------|
| MonoScene | 11.1 |
| MonoScene + Hierarchical Mamba module | 11.7 |

Table 6: Ablation study on MonoScene framework.

Therefore, reordering schemes that prioritize the z-axis allow Mamba to better capture spatial proximity information, leading to improved prediction performance.

Generalization. We apply our hierarchical Mamba module to the MonoScene(Cao and De Charette 2022) framework. Specifically, we replace the 3D voxel decoder in this framework with our implementation and train on 25% of the SemanticKITTI training set. As shown in Table 6, our Mamba module can improve the performance of MonoScene from 11.1% mIoU to 11.7% mIoU on SemanticKITTI val set.

Memory Usage and Inference Time. In Table 7, we present a comparative analysis of memory usage and inference time between OccMamba and M-CONet during both training and inference phases. The experiment is trained on 8 A40 GPUs and performed inference on a single RTX 4090 GPU. When the mamba feature dimension is set to 384, OccMamba demonstrates approximately a 20% reduction in memory usage during training and about a 30% reduction during inference compared to M-CONet. When the mamba feature dimension is reduced to 128, these reductions in-

| Method | Memory Usage(GiB) | | Inference Time(ms) | mIoU |
|--------------|-------------------|------------|--------------------|-------------|
| | Training | Inference | | |
| M-CONet | 37.3 | 12.1 | 416.0 | 20.5 |
| OccMamba-384 | 29.9 | 8.5 | 398.1 | 27.0 |
| OccMamba-128 | 19.2 | 6.2 | 235.7 | 25.9 |

Table 7: Comparison of memory usage and inference time. OccMamba-384 means OccMamba with mamba feature dimension being 384.

crease to approximately 49% for both training and inference memory usage. Besides, the inference time of OccMamba-128 is approximately half of the M-CONet and OccMamba-128 remarkably surpasses M-CONet in performance.

5 Conclusion

In this paper, we present the first Mamba-based network, termed OccMamba, for semantic occupancy prediction. To facilitate the processing of Mamba blocks and maximally retain the 3D spatial relationship, we design the Hierarchical Mamba Module. Our OccMamba is highly efficient and surpasses the previous state-of-the-art algorithms on three prevalent occupancy prediction benchmarks. As an innovative approach in this field, our OccMamba provides an effective means for handling large-scale voxels directly, and we believe it will inspire new advancements.

References

- Behley, J.; Garbade, M.; Milioto, A.; Quenzel, J.; Behnke, S.; Stachniss, C.; and Gall, J. 2019. Semantickitti: A dataset for semantic scene understanding of lidar sequences. In *Proceedings of the IEEE/CVF international conference on computer vision*, 9297–9307.
- Berman, M.; Triki, A. R.; and Blaschko, M. B. 2018. The lovasz-softmax loss: A tractable surrogate for the optimization of the intersection-over-union measure in neural networks. In *CVPR*, 4413–4421.
- Caesar, H.; Bankiti, V.; Lang, A. H.; Vora, S.; Liong, V. E.; Xu, Q.; Krishnan, A.; Pan, Y.; Baldan, G.; and Beijbom, O. 2020. nuscenes: A multimodal dataset for autonomous driving. In *Proceedings of the IEEE/CVF conference on computer vision and pattern recognition*, 11621–11631.
- Cao, A.-Q.; and De Charette, R. 2022. Monoscene: Monocular 3d semantic scene completion. In *Proceedings of the IEEE/CVF Conference on Computer Vision and Pattern Recognition*, 3991–4001.
- Chen, X.; Lin, K.-Y.; Qian, C.; Zeng, G.; and Li, H. 2020. 3d sketch-aware semantic scene completion via semi-supervised structure prior. In *Proceedings of the IEEE/CVF Conference on Computer Vision and Pattern Recognition*, 4193–4202.
- Dao, T.; Fu, D.; Ermon, S.; Rudra, A.; and Ré, C. 2022. Flashattention: Fast and memory-efficient exact attention with io-awareness. *Advances in Neural Information Processing Systems*, 35: 16344–16359.
- Gao, J.; Li, P.; Chen, Z.; and Zhang, J. 2020. A survey on deep learning for multimodal data fusion. *Neural Computation*, 32(5): 829–864.
- Garbade, M.; Chen, Y.-T.; Sawatzky, J.; and Gall, J. 2019. Two stream 3d semantic scene completion. In *Proceedings of the IEEE/CVF Conference on Computer Vision and Pattern Recognition Workshops*, 0–0.
- Gu, A.; and Dao, T. 2023. Mamba: Linear-time sequence modeling with selective state spaces. *arXiv preprint arXiv:2312.00752*.
- Gu, A.; Goel, K.; and Ré, C. 2021. Efficiently modeling long sequences with structured state spaces. *arXiv preprint arXiv:2111.00396*.
- He, K.; Zhang, X.; Ren, S.; and Sun, J. 2016. Deep residual learning for image recognition. In *Proceedings of the IEEE conference on computer vision and pattern recognition*, 770–778.
- Hilbert, D. 2013. *Dritter Band: Analysis· Grundlagen der Mathematik· Physik Verschiedenes: Nebst Einer Lebensgeschichte*. Springer-Verlag.
- Huang, Y.; Zheng, W.; Zhang, Y.; Zhou, J.; and Lu, J. 2023. Tri-perspective view for vision-based 3d semantic occupancy prediction. In *Proceedings of the IEEE/CVF conference on computer vision and pattern recognition*, 9223–9232.
- Li, J.; Han, K.; Wang, P.; Liu, Y.; and Yuan, X. 2020a. Anisotropic convolutional networks for 3d semantic scene completion. In *Proceedings of the IEEE/CVF Conference on Computer Vision and Pattern Recognition*, 3351–3359.
- Li, S.; Zou, C.; Li, Y.; Zhao, X.; and Gao, Y. 2020b. Attention-based multi-modal fusion network for semantic scene completion. In *Proceedings of the AAAI Conference on Artificial Intelligence*, volume 34, 11402–11409.
- Li, Y.; Ge, Z.; Yu, G.; Yang, J.; Wang, Z.; Shi, Y.; Sun, J.; and Li, Z. 2023a. Bevdepth: Acquisition of reliable depth for multi-view 3d object detection. In *AAAI*, volume 37, 1477–1485.
- Li, Y.; Yu, Z.; Choy, C.; Xiao, C.; Alvarez, J. M.; Fidler, S.; Feng, C.; and Anandkumar, A. 2023b. Voxformer: Sparse voxel transformer for camera-based 3d semantic scene completion. In *Proceedings of the IEEE/CVF conference on computer vision and pattern recognition*, 9087–9098.
- Liang, D.; Zhou, X.; Wang, X.; Zhu, X.; Xu, W.; Zou, Z.; Ye, X.; and Bai, X. 2024. PointMamba: A Simple State Space Model for Point Cloud Analysis. *arXiv preprint arXiv:2402.10739*.
- Lin, T.; Wang, Y.; Liu, X.; and Qiu, X. 2022. A survey of transformers. *AI open*, 3: 111–132.
- Lin, T.-Y.; Dollár, P.; Girshick, R.; He, K.; Hariharan, B.; and Belongie, S. 2017. Feature pyramid networks for object detection. In *Proceedings of the IEEE conference on computer vision and pattern recognition*, 2117–2125.
- Liu, J.; Yu, R.; Wang, Y.; Zheng, Y.; Deng, T.; Ye, W.; and Wang, H. 2024a. Point mamba: A novel point cloud backbone based on state space model with octree-based ordering strategy. *arXiv preprint arXiv:2403.06467*.
- Liu, Y.; Tian, Y.; Zhao, Y.; Yu, H.; Xie, L.; Wang, Y.; Ye, Q.; and Liu, Y. 2024b. Vmamba: Visual state space model. *arXiv preprint arXiv:2401.10166*.
- Liu, Z.; Tang, H.; Amini, A.; Yang, X.; Mao, H.; Rus, D. L.; and Han, S. 2023. Bevfusion: Multi-task multi-sensor fusion with unified bird’s-eye view representation. In *2023 IEEE international conference on robotics and automation (ICRA)*, 2774–2781. IEEE.
- Ma, Q.; Tan, X.; Qu, Y.; Ma, L.; Zhang, Z.; and Xie, Y. 2024. COTR: Compact Occupancy TRansformer for Vision-based 3D Occupancy Prediction. In *Proceedings of the IEEE/CVF Conference on Computer Vision and Pattern Recognition (CVPR)*, 19936–19945.
- Nguyen, E.; Goel, K.; Gu, A.; Downs, G.; Shah, P.; Dao, T.; Baccus, S.; and Ré, C. 2022. S4nd: Modeling images and videos as multidimensional signals with state spaces. *Advances in neural information processing systems*, 35: 2846–2861.
- Pan, J.; Wang, Z.; and Wang, L. 2024. Co-Occ: Coupling Explicit Feature Fusion with Volume Rendering Regularization for Multi-Modal 3D Semantic Occupancy Prediction. *IEEE Robotics and Automation Letters*.
- Pan, Y.; Gao, B.; Mei, J.; Geng, S.; Li, C.; and Zhao, H. 2020. Semanticpos: A point cloud dataset with large quantity of dynamic instances. In *2020 IEEE Intelligent Vehicles Symposium (IV)*, 687–693. IEEE.
- Rist, C. B.; Emmerichs, D.; Enzweiler, M.; and Gavrila, D. M. 2021. Semantic scene completion using local deep implicit functions on lidar data. *IEEE transactions on pattern analysis and machine intelligence*, 44(10): 7205–7218.

- Roldao, L.; de Charette, R.; and Verroust-Blondet, A. 2020. Lmscnet: Lightweight multiscale 3d semantic completion. In *2020 International Conference on 3D Vision (3DV)*, 111–119. IEEE.
- Roldao, L.; De Charette, R.; and Verroust-Blondet, A. 2022. 3D semantic scene completion: A survey. *International Journal of Computer Vision*, 130(8): 1978–2005.
- Shi, H.; Wang, S.; Zhang, J.; Yin, X.; Wang, Z.; Zhao, Z.; Wang, G.; Zhu, J.; Yang, K.; and Wang, K. 2024. Oc-cfiner: Offboard occupancy refinement with hybrid propagation. *arXiv preprint arXiv:2403.08504*.
- Tong, W.; Sima, C.; Wang, T.; Chen, L.; Wu, S.; Deng, H.; Gu, Y.; Lu, L.; Luo, P.; Lin, D.; et al. 2023. Scene as occupancy. In *Proceedings of the IEEE/CVF International Conference on Computer Vision*, 8406–8415.
- Vaswani, A.; Shazeer, N.; Parmar, N.; Uszkoreit, J.; Jones, L.; Gomez, A. N.; Kaiser, Ł.; and Polosukhin, I. 2017. Attention is all you need. *Advances in neural information processing systems*, 30.
- Vora, S.; Lang, A. H.; Helou, B.; and Beijbom, O. 2020. Pointpainting: Sequential fusion for 3d object detection. In *Proceedings of the IEEE/CVF conference on computer vision and pattern recognition*, 4604–4612.
- Wang, H.; Tang, H.; Shi, S.; Li, A.; Li, Z.; Schiele, B.; and Wang, L. 2023a. UniTR: A Unified and Efficient Multi-Modal Transformer for Bird’s-Eye-View Representation. In *Proceedings of the IEEE/CVF International Conference on Computer Vision*, 6792–6802.
- Wang, S.; Li, B. Z.; Khabsa, M.; Fang, H.; and Ma, H. 2020. Linformer: Self-attention with linear complexity. *arXiv preprint arXiv:2006.04768*.
- Wang, X.; Zhu, Z.; Xu, W.; Zhang, Y.; Wei, Y.; Chi, X.; Ye, Y.; Du, D.; Lu, J.; and Wang, X. 2023b. Openoccupancy: A large scale benchmark for surrounding semantic occupancy perception. In *Proceedings of the IEEE/CVF International Conference on Computer Vision*, 17850–17859.
- Xia, Z.; Liu, Y.; Li, X.; Zhu, X.; Ma, Y.; Li, Y.; Hou, Y.; and Qiao, Y. 2023. Scpnet: Semantic scene completion on point cloud. In *Proceedings of the IEEE/CVF conference on computer vision and pattern recognition*, 17642–17651.
- Yan, X.; Gao, J.; Li, J.; Zhang, R.; Li, Z.; Huang, R.; and Cui, S. 2021. Sparse single sweep lidar point cloud segmentation via learning contextual shape priors from scene completion. In *Proceedings of the AAAI Conference on Artificial Intelligence*, volume 35, 3101–3109.
- Yan, Y.; Mao, Y.; and Li, B. 2018. Second: Sparsely embedded convolutional detection. *Sensors*, 18(10): 3337.
- Zhang, S.; Zhai, Y.; Mei, J.; and Hu, Y. 2024a. FusionOcc: Multi-Modal Fusion for 3D Occupancy Prediction. In *ACM Multimedia 2024*.
- Zhang, Y.; Zhang, J.; Wang, Z.; Xu, J.; and Huang, D. 2024b. Vision-based 3D occupancy prediction in autonomous driving: a review and outlook. *arXiv preprint arXiv:2405.02595*.
- Zhang, Y.; Zhu, Z.; and Du, D. 2023. Occformer: Dual-path transformer for vision-based 3d semantic occupancy prediction. In *Proceedings of the IEEE/CVF International Conference on Computer Vision*, 9433–9443.
- Zhou, Y.; and Tuzel, O. 2018. Voxelnet: End-to-end learning for point cloud based 3d object detection. In *Proceedings of the IEEE conference on computer vision and pattern recognition*, 4490–4499.
- Zhu, L.; Liao, B.; Zhang, Q.; Wang, X.; Liu, W.; and Wang, X. 2024. Vision mamba: Efficient visual representation learning with bidirectional state space model. *arXiv preprint arXiv:2401.09417*.